Based on auxetic foam: A novel type of seismic metamaterial for Lamb waves

Ting Ting Huang, Yi Zeng, Xin Ren, Yi Zhang, Chen Luo, Xiang Yu Zhang, Yi Min Xie

Based on auxetic foam: A novel type of seismic metamaterial for Lamb waves

Ting Ting Huang[a], Yi Zeng[b,c], Xin Ren[a,*], Yi Zhang[a], Chen Luo[a], Xiang Yu Zhang[a], Yi Min Xie[d]

[a] *College of Civil Engineering, Nanjing Tech University, Nanjing, Jiangsu, 211816, PR China*

[b] *Department of Mechanics, School of Mechanical Engineering, Tianjin University, Tianjin, 300350, China*

[c] *Université de Lorraine, CNRS, Institut Jean Lamour, Nancy 54000, France*

[d] *Centre for Innovative Structures and Materials, School of Engineering, RMIT University, Melbourne, 3001, Australia*

* Corresponding author: Xin Ren. Email: xin.ren@njtech.edu.cn

ABSTRACT

Seismic metamaterial (SM) has lately received significant attention in the field of vibration isolation and damping due to its wave manipulation and bandgap properties. However, the limitations of unit cell size and the difference of the material parameters of each component have made it challenging to generate an ultra-low frequency bandgap. In order to overcome this challenge, a novel type of 2D SM composed of auxetic foam and steel is proposed to attenuate seismic waves at ultra-low frequencies. Firstly, the band structure of the SMs and the vibration modes of the upper and lower bounds of the first complete bandgap are calculated and analyzed by using the finite element method, and the mechanism of the bandgap generation is clarified. The transmission spectrum under the Lamb wave incident on the SM is investigated. It is validated that Lamb waves have a good attenuation effect in the frequency range below 10 Hz. Secondly, a parametric study of the SM with auxetic foam-coated hollow steel columns is carried out. The numerical results show that the shape and height of the unit cell, the elastic modulus, density and Poisson's ratio of the auxetic foam play important roles in the formation of the bandgap. Finally, the numerical simulation verifies that adding through holes in the matrix which reduces the equivalent mass density of the matrix could widen the bandgap and enhance the effective attenuation of seismic waves. Based on theoretical model and combined with the exceptional material characteristics of auxetic foam, the focus of the study is to achieve a wide bandgap coverage for the seismic peak spectrum of 2 Hz which causes the principal damage of surface buildings.

Keywords: Auxetic, Negative Poisson's ratio, Bandgap, Seismic metamaterial, Vibration isolation, Phononic crystals, Ultra-low frequency

1. Introduction

Earthquakes and the secondary disasters caused by earthquakes are extremely destructive, especially the collapse of buildings is one of the most important reasons for casualties and major property losses. Therefore, improving the seismic performance of buildings and effectively reducing this type of hazard has become an urgent task and a popular research topic. The seismic performance of a structure depends on its mass, strength, deformability, and damping [1]. To ensure the safety of the main structure, the conventional method of damping and dissipating energy is to direct the energy input from the earthquake to a specific energy-consuming device, which is equivalent to increasing the damping of the structure. However, the energy dissipation elements are often integrated with the main structure, which easily causes excessive lateral deformation and residual deformation of the main structure [2,3]. Residual deformation has a serious impact on the seismic performance of structures that are about to collapse or may experience subsequent earthquakes. Furthermore, excessive residual deformation may cause the repair cost to exceed the reconstruction cost, resulting in a considerable economic loss [4-6]. The seismic metamaterials (SMs) [7-9] proposed in recent years pave a new way to prevent this from happening.

Metamaterials [10-12] are a novel type of material with artificial structure, which has special properties that natural materials do not have in nature. Metamaterials have many counterintuitive properties, such as negative refraction [13,14], frequency bandgaps [15-17], cloaking [18,19], negative Poisson's ratio [20-22], etc. In just over a decade, the concept of metamaterials has gradually penetrated to the materials science, magnetism, mechanics, thermotics and other disciplines. In 2010, it was rated as one of the top ten scientific and technological breakthroughs affecting mankind in the 21st century by Science magazine [23,24]. According to the different regulated elements, metamaterials can be divided into photonic metamaterials, mechanical

metamaterials and acoustic metamaterials, etc. Among them, photonic metamaterials are man-made structures composed of tailored micro-or nanostructured metallodielectric subwavelength building blocks. Mechanical metamaterials are artificial micro-structures designed to regulate elastic waves. Their novel properties often depend on the structure rather than just the composition of the material [25,26]. To date, common metamaterials include: left-handed materials, photonic crystals, phononic crystals, zero refractive index materials, gradient refractive index materials, etc. Phononic crystals [27-30] are periodic composites with elastic bandgaps composed of two or more types of elastic media. One of the prominent characteristics is the separate bands in the elastic wave dispersion. As a result, the stop bands or band gaps will be generated, in which the elastic wave cannot propagate. The bandgap characteristics of phononic crystals have potential applications in the field of vibration isolation and damping.

SMs are based on the local resonance theory of phononic crystals [31,32], and exploited the bandgap characteristics of phononic crystals to control seismic waves [33]. In 2000, Liu *et al.* [34] creatively proposed the concept of locally resonant phononic crystals, which can generate very low frequency bandgaps under the condition of small size, greatly breaking through the limitations of traditional phononic crystals. Later, to further validate that the small-sized metamaterials can control long-wavelength seismic waves, Brule *et al*. [35] conducted seismic wave experiments with periodic drilling holes on the ground. Huang *et al.* [36] studied the periodic columns and periodic wave barrier structures in civil engineering, and proved the strong attenuation in the bandgap through simulation. Yan *et al.* [37] proposed seismic metamaterials based on Lamb wave theory and conducted experiments. Colombi *et al.* [38] found that the super-large local resonance structure composed of forest and soil could produce two bandgaps with a wide frequency range. Subsequently,

various SMs that open the bandgap in a low frequency range based on local resonance have been extensively studied and experimentally verified [39-41]. In almost all the studies, the main damage to a building is the seismic wave with a frequency of 0.1-20 Hz [42-44]. Among them, to shield the frequency spectrum of the peak seismic wave (about 2 Hz) that causes damage to the surface buildings remained a prime objective [45,46].

Simple mechanical and thermodynamical models, which show auxetic behavior, were found in the 80s of the 20th century[23,47,48]. Auxetic materials have unusual geometrical and mechanical characteristics such as high shear stiffness, indentation resistance, improved damping and sound absorption properties[49-53]. Strek *et al*. [54] proposed that auxetic material and structures or composite with auxetic layer have better damping properties than materials with positive Poisson's ratio. Bianchi *et al*. [55] described the vibration transmissibility behavior in conventional and auxetic foams under low and high amplitude vibrations. For the bandgap characteristics of auxetic materials, Ungureanu *et al*. [56] reported that the propagation of seismic waves with frequencies ranging from 1 Hz to 40 Hz can be influenced by a decameter scale version of auxetic-like metamaterials buried in the soil. D'Alessandro *et al.* [57] obtained a single periodic structure with a 3D wide adjustable bandgap by appropriately combining the auxetic properties of negative Poisson's ratio and the bandgap properties of phononic crystals. Bruggi *et al.* [58] investigated that directional and full band-pass filters are found in the case of micro-structures, and the auxetic behavior is caused by the rotational deformation of the periodic unit cell. However, there are still some deficiencies in the application of auxetic materials in vibration reduction, especially in all-direction wide bandgap in the ultra-low frequency band.

In this paper, a new 2D SM consisting of auxetic foam and steel composition is proposed to

achieve an ultra-low frequency bandgap. With the adjustable Poisson's ratio, elastic modulus and density of auxetic foam, the bandgap range of phononic crystal can be changed to absorb seismic waves with different frequencies and real-time changes. The specific contents are as follows: taking auxetic foam as matrix and hollow steel columns as scatterers, the periodic hollow steel columns (fillable concrete) are added into the matrix in order to calculate the band structure of the 2D SMs. The wave propagation in the plane perpendicular to the column is studied by finite element method, the bandgap characteristics are analyzed, and various factors affecting the bandgap characteristics are discussed in detail. The calculation of the transmission spectrum also verifies that the seismic wave is strongly and effectively attenuated in the bandgap, particularly in the range of 0.1-10 Hz, which is of great significance for the protection of important civil buildings. This study could open up new perspectives in the field of civil engineering and in related areas of ultra-low frequency vibration-damping protection.

2. Methods and models

In this paper, a new 2D SM composed of auxetic foam and steel is proposed to achieve the attenuation of Lamb waves, and the finite element method is used to numerically study its performance. As schematically shown in Fig. 1(a), a is the lattice constant and the height is h. The outer side-length and inner side-length of the hollow square steel column are denoted by b and c, where $b = 0.85a$ and $c = 0.4a$. Each metamaterial consists of hollow square steel column embedded in auxetic foam periodically arranged in the x-y directions. The auxetic foams used in this research were manufactured using open cell polyurethane foam through a thermo-mechanical process, and the main skeleton is a reticular structure [59,60]. The structure in Fig. 1(b) is obtained by filling the hollow column in Fig. 1(a) with a concrete inclusion. Fig. 1(c) shows a representative unit cell of the

corresponding reciprocal space. The blue, grey and green areas in Figs. 1(a-b) represent auxetic foam, steel and concrete, respectively. The corresponding material properties [61] and geometrical parameters of the unit cell are illustrated in Tables I and II, respectively.

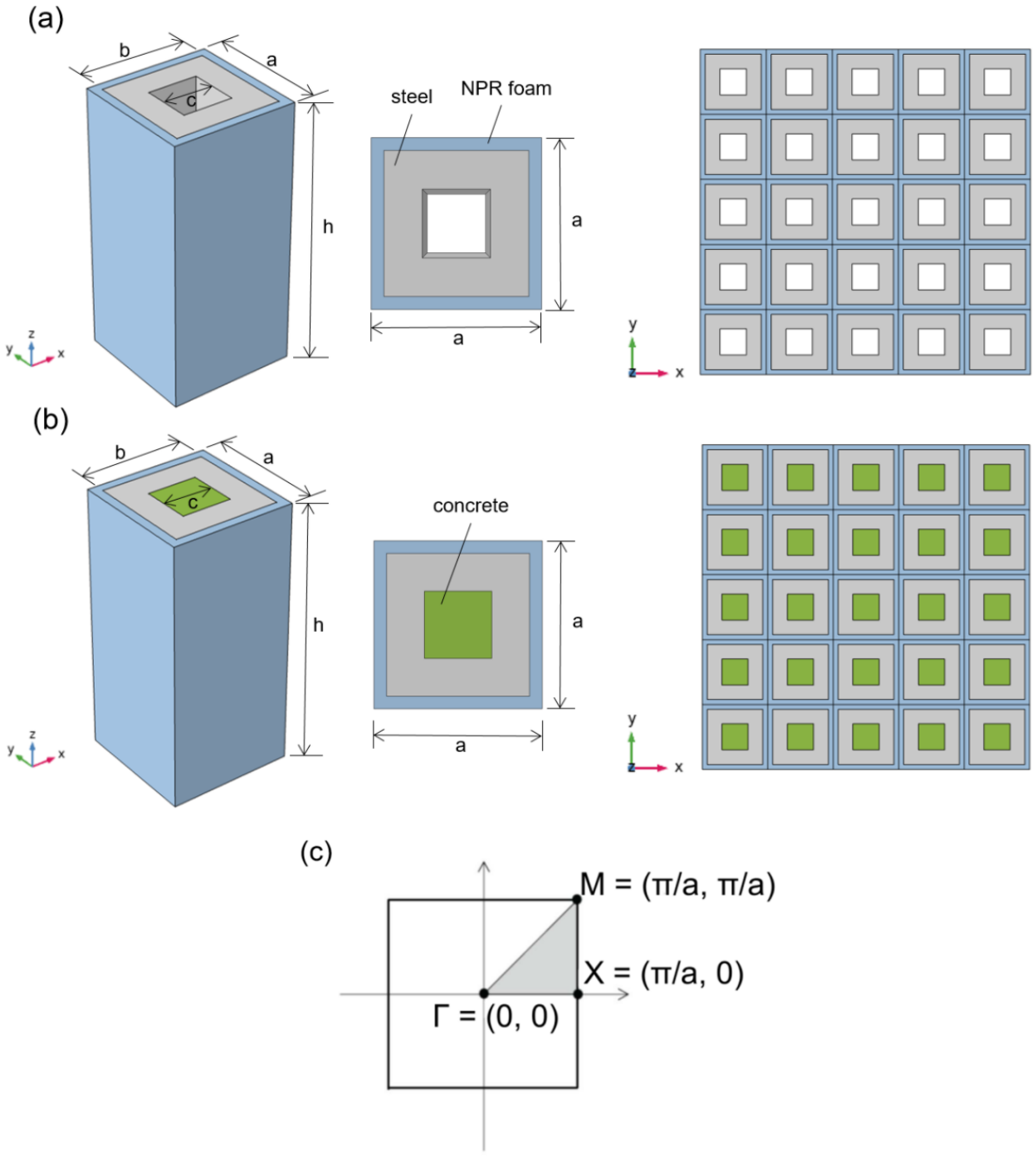

Fig. 1. Schematic representation of the SM structure: (a) unit cell and arrays composed of auxetic foam and hollow square steel column; (b) unit cell and arrays of concrete-filled column; (c) The First Irreducible Brillouin Zone (FIBZ) (the grey triangle of vertices Γ-X-M-Γ) for a square arrangement of inclusions.

Table I

Material parameters of unit cell.

Material	Density (kg/m^3)	Young's modulus (Pa)	Poisson's radio
Concrete	2500	4×10^{10}	0.3
Steel	7784	2.07×10^{11}	0.3
Auxetic foam	120	2.5×10^{4}	-0.8

Table II

Geometric parameters of unit cell.

a (m)	b (m)	c (m)	h (m)
10	8.5	4	20

For a square lattice of inclusions as in Fig. 1(c), the eigenmodes are evaluated for the wave vectors along the Γ-X-M-Γ directions of the highest symmetry of the Brillouin zone. Here we assume that the materials are linearly elastic, homogeneous, and isotropic, the governing equation for the in-plane wave propagation can be expressed as [62]

$$\nabla\cdot[\mathbf{C}(\mathbf{r}):\nabla\mathbf{u}]=\rho(\mathbf{r})\frac{\partial^2\mathbf{u}}{\partial t^2} \tag{2.1}$$

where $\mathbf{C}(\mathbf{r})$ and $\rho(\mathbf{r})$ are the elastic tensor and mass density tensor of the material, respectively; $\mathbf{r}$ = (x, y, z) is location vector; the vector $\mathbf{u}=(u_x,u_y,u_z)$ is the displacement vector; $\nabla=(\partial/\partial x,\partial/\partial y,\partial/\partial z)$ is the differential operator; "·", "**:**" denote the vector dot product and double-dot product of two dyadic, respectively; t is the time variable.

To determine the band structure of metamaterials with infinite periodic structure, the periodic cell analysis and the Bloch periodic boundary conditions covering a certain range of wave vectors are needed to solve the wave equation by using the finite element software. A relatively small range of wave vectors can cover the edge of the FIBZ. According to Floquet-Bloch theorem, calculations can be performed within FIBZ. After dividing the mesh with finite elements, the eigenvalue equation

of the discrete form of the unit cell can be expressed as

$$\left(\mathbf{K}-\omega^2\mathbf{M}\right)\cdot\mathbf{U}=0 \tag{2.2}$$

where **K** is the stiffness matrix and **M** is the mass matrix, which are the functions of the wave vector **k**. ω is angular frequency. According to Floquet-Bloch theorem of wave propagation in periodic structure [63], the wave field should have the following form

$$\mathbf{u}\left(\mathbf{r},t\right)=e^{i\left(\mathbf{k}\cdot\mathbf{r}-\omega t\right)}\mathbf{u}_{\mathbf{k}}\left(\mathbf{r}\right) \tag{2.3}$$

where $\mathbf{u}_{\mathbf{k}}(\mathbf{r})$ is displacement modulation function, $i=\sqrt{-1}$, **k** is the wave vector. It can be seen from equation (2.3) that Bloch periodic boundary conditions should be set on the bound of the unit cell to solve equation (2.1), which is the displacement amplitude condition

$$\mathbf{u}\left(\mathbf{r}+\mathbf{a},t\right)=e^{i\left(\mathbf{k}\cdot\mathbf{a}\right)}\mathbf{u}\left(\mathbf{r},t\right) \tag{2.4}$$

where **a** is the lattice translation vector. Simultaneous equations (2.2) and (2.4) can be used to solve the eigenfrequency under the given wave vector **k**.

In this paper, the commercial finite element software COMSOL Multiphysics 5.4 is used to solve the eigenvalue equation and band structure. By substituting the characteristic frequency into the governing wave equations (2.2), the corresponding eigenmode can be obtained. The band structure can be obtained by sweeping the corresponding FIBZ of the wave vector **k**.

3. Results and discussionf

3.1 Band structure

For specific geological configurations, such as a deep layer with a smaller shear-wave velocity compared to that in overlying layers, a substantial part of the seismic energy can be propagated in the stiffer layer in the form of guided or Lamb waves [64]. Firstly, the band structure of this kind of

SM is calculated by numerical simulation. The unit cell composed of auxetic foam and hollow square steel column is selected, in which the periodic boundary conditions are applied to the four vertical planes of the unit cell. The top and bottom boundary conditions are set as free boundary conditions. Fig. 2(a) shows the band structure of SM with auxetic foam-coated hollow steel columns based on a plate structure environment. It could be seen that the first complete bandgap, with a width of 5.555 Hz from 0.515 Hz to 6.070 Hz, is exhibited between the sixth band and the seventh band. To better illustrate the bandgap property, an important parameter of relative bandwidth is defined as $2(f_u - f_l)/(f_u + f_l)$, with f_u and f_l being the frequencies of the upper and lower boundaries of the BG, respectively [41]. By calculation, the relative bandwidth of the SM is as high as 1.687, which means that it can satisfy the broader seismic demand. Since the ninth and tenth bands are flat, it can be considered that the second, third, and fourth bandgaps are merged into a large complete bandgap. Thus, the bandgap range of the SM is between 0.515 Hz and 6.575 Hz, and seismic waves in this frequency range cannot propagate through the SM. It is worth noting that the bandgap produced by this novel type of 2D SM contains the main peak spectrum frequency 2 Hz that causes seismic damage, which can effectively attenuate seismic waves.

A square column filled with a concrete inclusion was designed and studied as shown in Fig.1(b), and the corresponding band structure is illustrated in Fig. 2(b). It could be seen that the first complete bandgap lies between the sixth and seventh bands, and the frequency ranges from 0.511 Hz to 6.070 Hz. Similarly, since the ninth band and the tenth band are horizontal, the second, third, and fourth complete bandgaps can be superimposed to a wider complete bandgap which extends from 6.071 Hz of the eighth band to 6.757 Hz of the eleventh band. In addition, it is also found that the location where the complete bandgaps of the concrete-filled column appear is almost the same as

that of the non-filled structure (Figs. 2(a-b)).

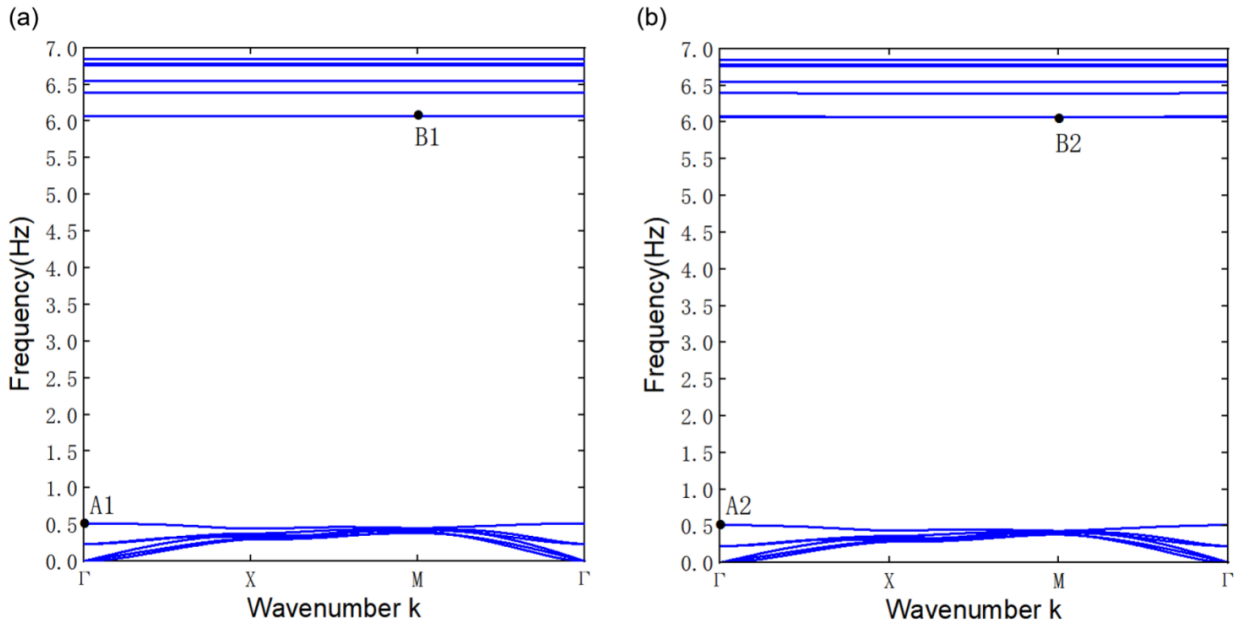

Fig. 2. Band structure for Lamb waves: (a) hollow square column; (b) concrete-filled square column.

3.2 Vibration modes

In order to investigate the generation mechanism of the bandgaps for plate-like SMs, the vibration modes of the upper and lower bounds of the first complete bandgap were calculated. The results are as shown in the figure: Figs. 3(a-b) show the vibration modes of the lower and upper bounds of the first bandgap of the hollow square column (Fig. 2(a)), and the upper and lower bounds of the bandgap take points B1 and A1 respectively; Figs. 3(c-d) respectively show the vibration modes of the lower and upper bounds of the first complete bandgap of the concrete-filled column (Fig. 2(b)), and the upper and lower bounds of the bandgap are taken as points B2 and A2, respectively. It can be seen from the figure that the square lattice of these structures can be regarded as the periodic arrangement of the scatterers (steel part) connected by the connectors (auxetic foam part). At the lower bound of the complete bandgaps, as shown in Fig. 3(a) and Fig. 3(c), the

vibration is mainly concentrated on the scatterers, and the connectors act as springs between the neighboring scatterers. For the upper bound of the complete bandgaps, as shown in Fig. 3(b) and 3(d), the vibrations are mainly concentrated on the connectors, while the scatterers barely vibrate.

The lower bound (A1) corresponding to Fig. 3(a) was analyzed. It could be seen that the scatterer rotates around the central axis, while the connectors of adjacent units have obvious anti-phase vibration around the scatterer, and the middle of the connector is almost motionless. At the upper bound (B1) shown in Fig. 3(b), the scatterer remains stationary and the connector vibrates in the *z*-axis direction. Figs. 3(c-d) show the vibration modes of the lower bound (A2) and upper bound (B2) of the first complete bandgap of the concrete-filled column. Obviously, the vibration mode of the structure filled with concrete is similar to that of the structure without concrete, because the combination of steel and concrete is equivalent to a scatterer. Here, the auxetic foam still acts as a spring, while the low frequency wide bandgap is due to the existence of local resonance units in the structure. Both the similarity of band gap and the similarity of vibration modes are beneficial to the practical application of structures. For example, the concrete-filled columns can be constructed as the lower foundation of buildings when attenuating seismic waves, while hollow square columns can be built around buildings to save material costs.

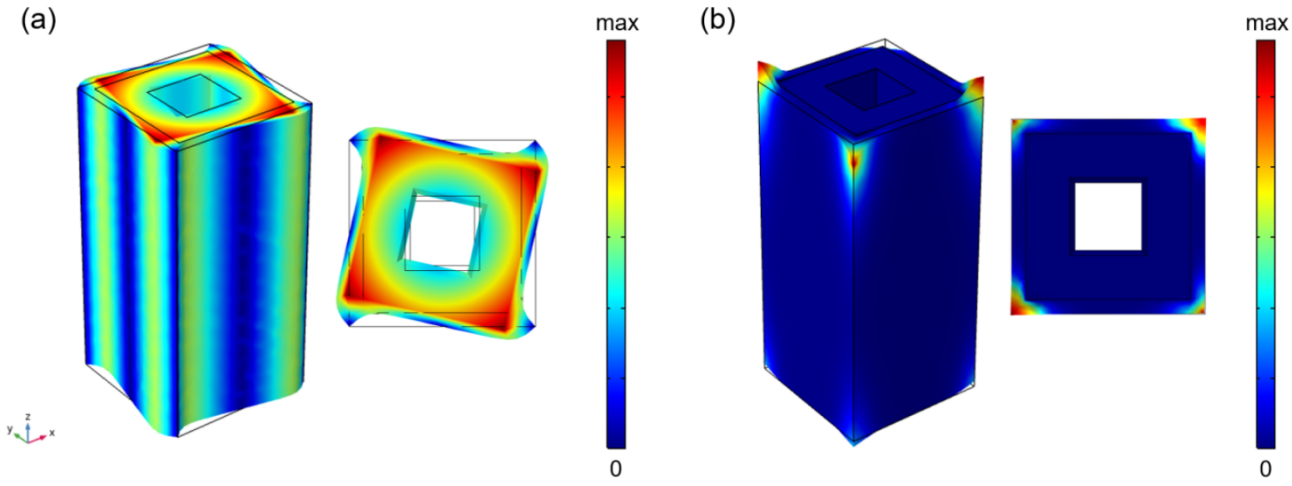

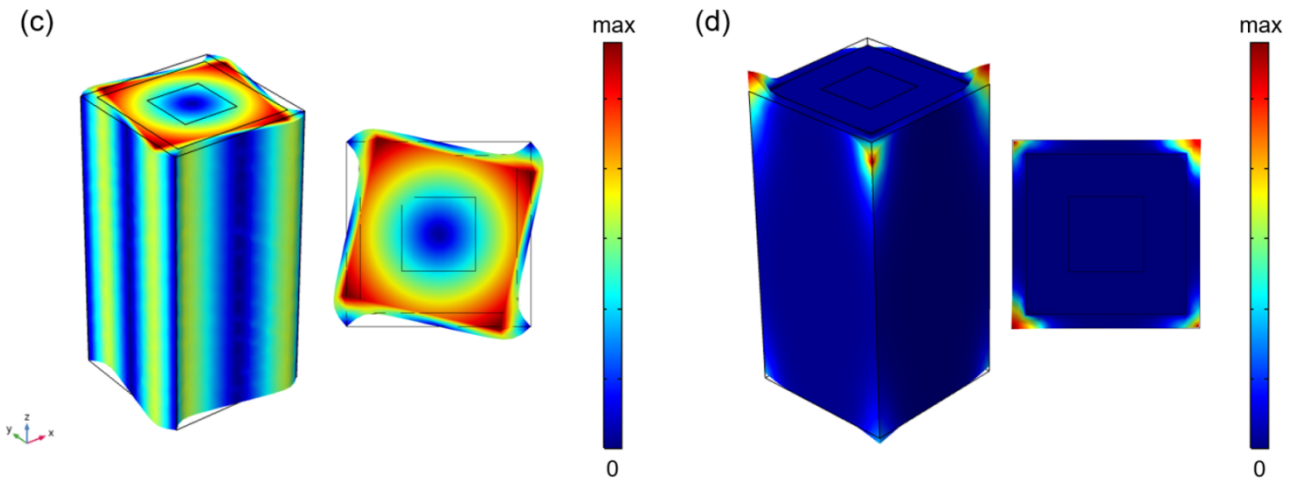

Fig. 3. The vibration modes at the first complete bandgaps: (a) A1 point at 0.515 Hz; (b) B1 point at 6.070 Hz; (c) A2 point at 0.511 Hz; (d) B2 point at 6.070 Hz. The color indicates the total displacement (u) ranging from 0 to maximum.

3.3 Frequency domain analysis

The band structure and bandgap of 2D SMs are calculated based on the infinite unit cell model. Although the position and width of bandgap can be explained, the damping effect of finite period structure cannot be fully reflected. Obviously, in practice all periodic structures are finite. To validate the accuracy and performance of bandgap, a finite SM system based on transmission spectrum analysis is performed. The SM system is composed of auxetic foam-coated hollow square columns arranged periodically. Through the observation of the displacement field of the SM, the position and width of the bandgap are validated, which further proves that the SM proposed could shield seismic waves.

The commercial finite element software COMSOL Multiphysics 5.4 was used to calculate the frequency domain of the SM system composed of 6 unit cells. The parameters of the unit cell were consistent with those shown in Table 1 above. Low reflection boundary conditions or perfectly matched layers were applied at both ends of the x- direction to prevent the reflection of waves from the bound, and periodic boundary conditions were applied along the y- direction. Firstly, an incident

surface waves with polarizations along *x*-*y*-*z* directions is applied at the interface between the low reflection boundary and the homogeneous part on the left side of the SM. The acceleration A1 behind the SM is then collected, and the acceleration A0 is collected at the same acquisition point when there is no SM. Finally, as shown in Fig. 4(a), perform a frequency sweep analysis on the frequency range from 0 Hz to 7 Hz (excluding 0 Hz) to calculate the transmission coefficient. In the result, the data of acceleration A1 and A0 are derived respectively, and the transmission spectrum calculation formula is set to $TS = 20 \times \log_{10}(A_1 / A_0)$, processing through Matlab or Origin can obtain the result of transmission spectrums. Fig. 4(a) shows the transmission spectrums of the 2D SM. It can be found that there is a large attenuation in the frequency range of 0.515 - 6.070 Hz, which basically coincides with the first bandgap of the band structure. The transmission characteristics in this region have an average attenuation of over 200 dB, and the maximum attenuation intensity reaches 352 dB, which has excellent shock absorption characteristics.

To further validate the shielding capability of the SM proposed, the total displacement of the incident wave when vibrating at two frequency points inside the bandgap and outside the bandgap are given, respectively, as shown in Figs. 4(b-c). It could be found that at 0.34 Hz outside the bandgap (Fig. 4(b)), the incident wave is partially reflected, but some of it still passes through the SM. It can be found that the matrix vibration at this time is slightly larger than the scatterer. However, when the frequency is 3.5 Hz in the bandgap (Fig. 4(c)), the incident wave is almost completely reflected and confined to the soil on the left. This can be explained that under the excitation of the elastic wave of a specific frequency, each scatterer resonates and interacts with the elastic wavelength wave traveling wave to restrain its propagation. Hence, this SM can provide an area with almost no Lamb waves interference.

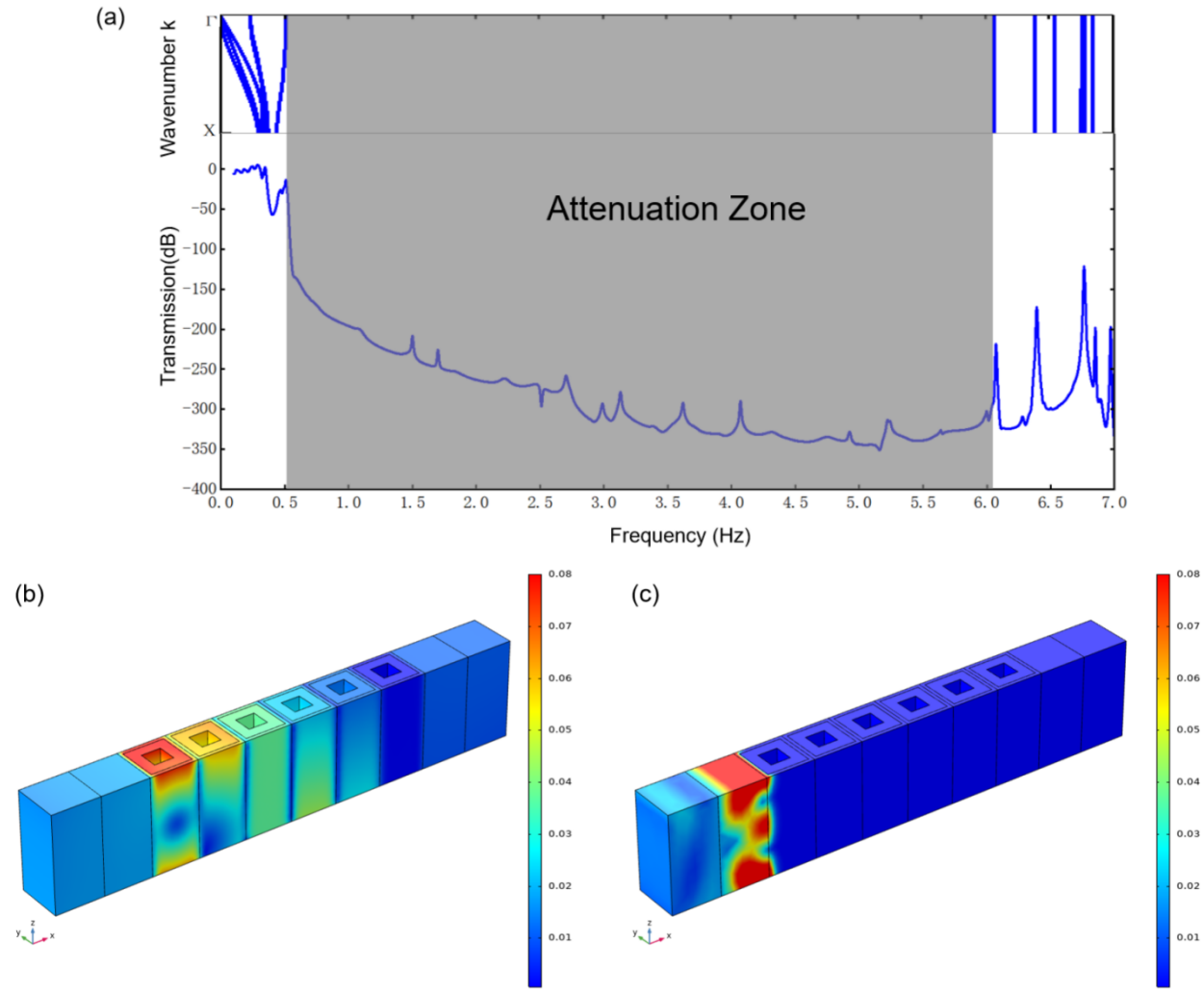

Fig. 4. Frequency domain analysis for the 2D SM with 6 unit cells: (a) Transmission spectrum in the frequencies range of 0 Hz-7.0 Hz; (b) The total displacement field with frequencies of 0.34 Hz and (c) 3.5 Hz. The color legends represent the displacement amplitude. (Highlighted grey region indicates attenuation zone that coincides with the first bandgap in the ΓX direction.)

3.4 Effect of geometric parameters

From the analysis above, it could be seen that the generation of the ultra-low frequency complete bandgap is due to the presence of local resonance units in the structure. To further illustrate the mechanism of the local resonance bandgap, the variation of the bound frequency of the plate structure shown in Fig. 2(a) with the change of a single parameter is investigated in Fig. 5.

Fig. 5(a) shows the calculation results obtained by changing only the outer side-length *b* of the hollow square steel column while keeping the lattice constant *a* and the inner side-length *c* unaltered.

Fig. 5(b) shows the influence of different height *h* on the bound frequency of the first bandgap when other parameters remain the same as previously mentioned. In Fig. 5(a), it is obvious that the complete bandgap widens and shifts toward higher frequencies with the increase of *b/a*. Since the upper bound frequency of the bandgap increases monotonously, while the frequency of the lower bound is basically unaltered, the width of the bandgap increases. This property can be used to realize a highly efficient rainbow trapping effect. In Fig. 5(b), it is interesting to note that the height of the unit cell influences inhibited frequencies than other considered parameters. With the increase of *h/a*, the lower bound frequency and the upper bound frequency of the first complete bandgap are almost unaltered, which is a critical feature of SMs with local resonant bandgaps. In other words, when the filling rate remains unaltered, different heights may have little effect on the first bandgap start-stop frequency or on the ultra-low bandgap start-stop frequency. Hence, the specific dimensions of seismic metamaterial unit cells could be chosen based on the practical application and the resulting maximal threat wavelength.

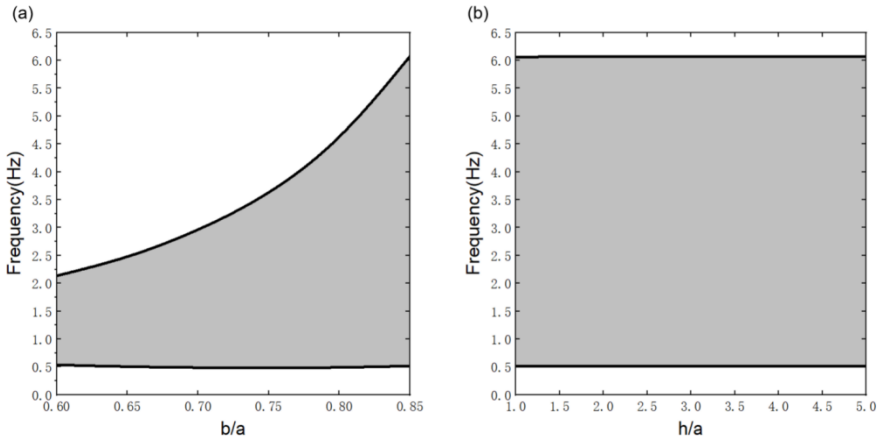

Fig. 5. The lower bound frequency and the upper bound frequency of the first complete bandgap for the SM as the ratio of (a) *b/a*; (b) *h/a*. (The grey region represents the first complete bandgap.)

3.5 Effect of material parameters

The bandgap width and frequency of upper and lower bounds are closely related to the material

properties. In previous section, the relationship between the first complete bandgap and geometric parameters was discussed. In this section, the influence of the elastic parameters of auxetic foam on the first complete bandgap was mainly discussed, and the shaded part represented the first complete bandgap. Existing studies have found that by changing the size and volume compression ratio of conventional foams, a series of auxetic foams with different auxetic effects can be made. Meanwhile, the corresponding Young's modulus and density also change accordingly. The Young's modulus E, density ρ and Poisson's ratio v of auxetic foam are usually varied in the range of 5~25 kPa, 75~120 kg/m^3 and -1.5~0 [59,60,65,66]. In order to compare the effect of positive and negative Poisson's ratio on the resonance structure, the value range of Poisson's ratio is set as -0.8~0.4. Similarly, based on the above-mentioned SM unit cell to ensure that other factors remain unaltered, the changes of Young's modulus E, density ρ and Poisson's ratio v on the bandgap are discussed respectively.

Fig. 6(a) shows the width variation of the first complete bandgap for different values of Young's modulus. When Young's modulus of auxetic foam increases from 5 kPa to 25 kPa, the lower bound frequency of the bandgap rises slowly, while the bandgap sizes are enlarged due to the rapidly shift of pass bands towards higher frequencies. This occurs due to the increase of the matrix stiffness, resulting in corresponding changes of the mode shapes. It is worth noting that reducing the stiffness of the matrix can reduce the bandgap frequency. The influence of the matrix density on the width of the first complete bandgap is shown in Fig. 6(b). When the density of the auxetic foam increases from 75 kg/m^3 to 120 kg/m^3, the complete bandgap decreases gradually and steadily shifts to a lower frequency range. Although the lower bound of the bandgap remains almost unaltered, the width of the bandgap becomes narrower because the upper bound of the bandgap shifts to a lower frequency.

As can be seen from Fig. 6(c), when the Poisson's ratio increases from -0.8 to 0.4, the upper

bound frequency declines rapidly. In contrast, the lower bound has different changes. When the Poisson's ratio increases from -0.8 to 0.2, the lower bound of the bandgap decreases slowly; and the lower bound increases slightly with the Poisson's ratio increasing from 0.2 to 0.4. In general, the complete bandgap width decreases gradually. It can be predicted that the complete bandgap will eventually close with the Poisson's ratio continues to increase. In summary, material parameters such as Young's modulus E, mass density ρ, and Poisson's ratio v have a significant effect on the width and location of the complete bandgap.

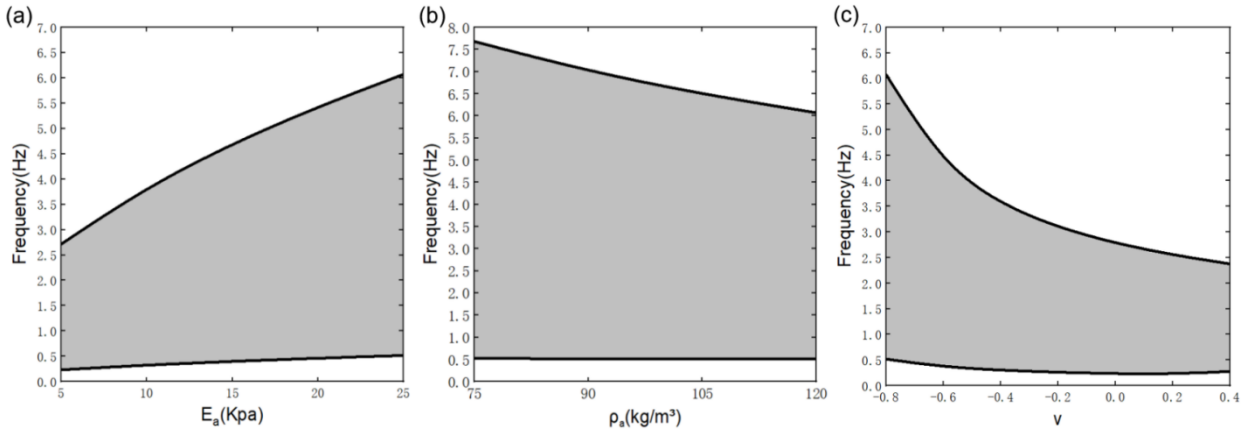

Fig. 6. Effect of different material parameters of auxetic foam on the first complete bandgap: (a) the Young's modulus E; (b) the mass density ρ; (c) the Poisson's ratio v. (The grey region represents the first complete bandgap.)

3.6 Effect of equivalent mass density of matrix

In addition, the effect of the equivalent mass density of matrix on the first bandgap frequencies was analysed. Seen from Fig. 6(b), the lower bound frequency is basically independent of the characteristics of the matrix material, while the upper bound frequency only decreases with the increase of the density of the matrix material. This occurs due to the increase of the equivalent mass of the matrix, resulting in a decrease in the characteristic frequency of the vibration mode corresponding to the upper bound of the bandgap. Therefore, in order to obtain a wider bandgap, the original structure was optimized. As shown in Fig. 7(a), ensuring that other parameters remain

unaltered, a small hole with a radius of r = 0.8 m is dug at each of the four corners of the unit cell to reduce the equivalent density of the matrix. Simulations show that the frequency range of the first complete bandgap of the optimized structure is 0.505-7.341 Hz shown in Fig. 7(b), the relative bandwidth is 1.743. Owe to the upper bandgap of the first complete bandgap increases, and the lower bandgap is almost unaltered, the relative bandwidth of the first bandgap has increased significantly by about 3.3% compared with the original structure in Fig. 2(a). The attenuation area of the optimized structure in Fig. 7(c) completely coincides with the bandgap of the band structure in Fig. 7(b), wherein the attenuation intensity is significantly increased compared to the previous one by comparing with the transmission spectrum of the original structure. Furthermore, the transmission spectrum of the SM composed of a single auxetic foam was also simulated. The results indicate that the SM has almost no attenuation to the Lamb wave below 7.5 Hz, which means the SM has no ultra-low frequency bandgap.

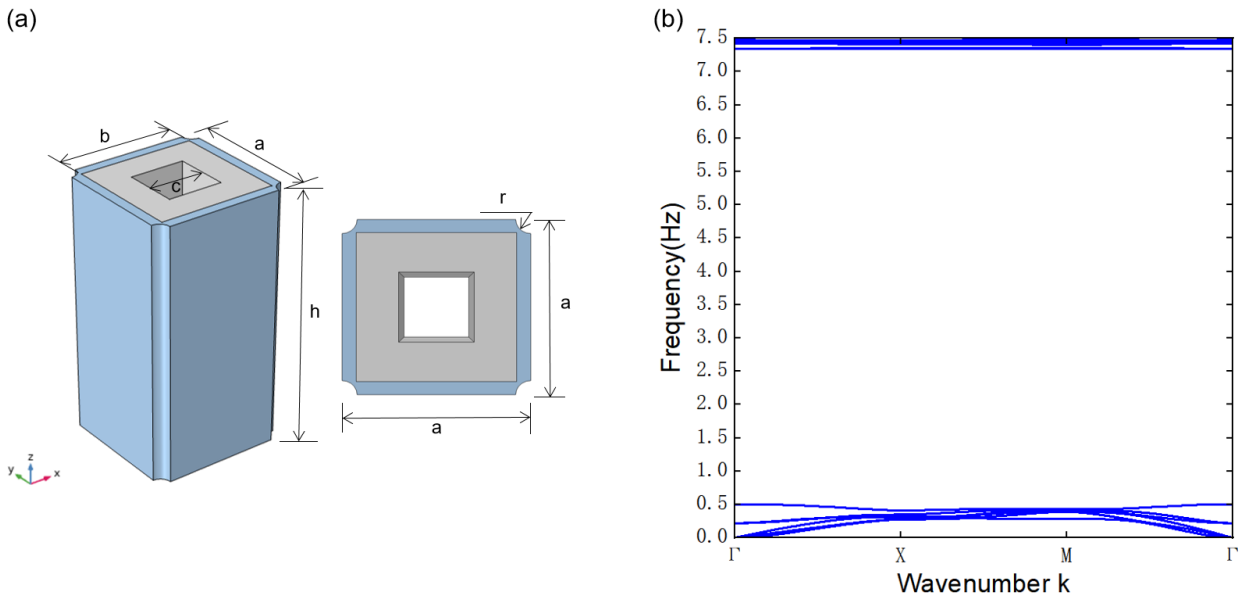

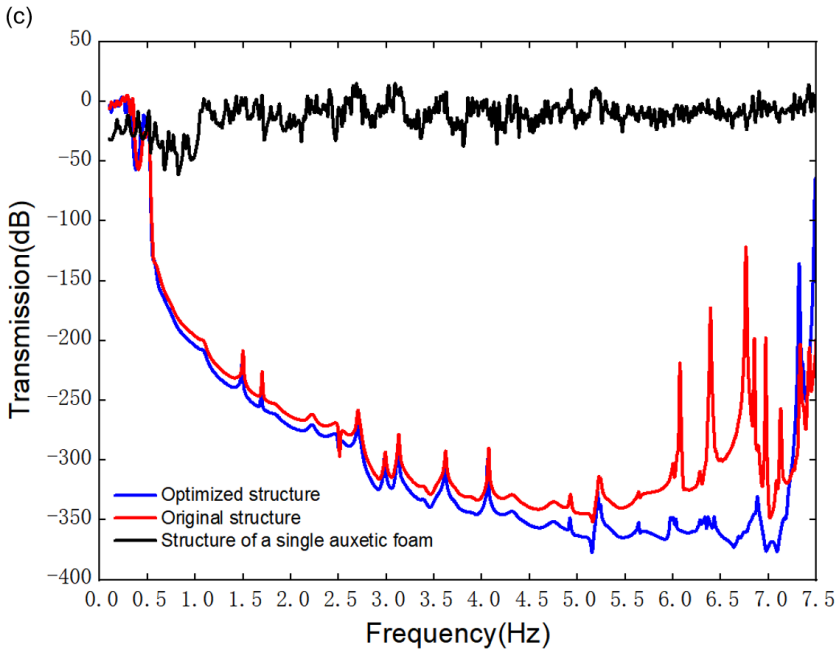

Fig. 7. Effect of the equivalent mass density of matrix on the first bandgap frequencies: (a) Optimized structure after digging small holes in the four corners of the unit cell; (b) Band structure for optimized structure; (c) Transmission spectrums in the ΓX direction of optimized structure, original structure, and structure of a single auxetic foam.

4. Conclusion

In summary, a novel type of 2D seismic metamaterial (SM) composed of auxetic foam and steel is proposed for the first time. It is noted that the 2D SM can effectively attenuate seismic waves, resist seismic wave peaks and reduce the damage to buildings due to its wide bandgap and ultra-low frequency. By utilizing the commercial finite element software COMSOL Multiphysics, the band structure of the SM plate is systematically studied. Simulations show that the SM plate generates a complete bandgap between 0.515 Hz and 6.070 Hz, including 2 Hz of the main wave peaks causing earthquake damage. The vibration modes at the upper and lower bounds of the first complete bandgap are calculated to examine the generation mechanism of the bandgap. It is found that the generation of the ultra-low frequency bandgap is due to the existence of local resonance elements in the structure. The transmission spectrum calculation proves that the structure has a good attenuation effect in the corresponding frequency range. Moreover, with the variation in geometrical parameters

and change in material properties of the auxetic foam, the bandgap width and location would change. By adding small holes in four corners of the matrix, it is proved that reducing the equivalent mass density of the matrix can widen the bandgap width and enhance the effective attenuation in the local resonant bandgap. This study manifests that the proposed SM can attenuate seismic waves in the frequency range of its ultra-low bandgap to protect important civil buildings from earthquake hazards.

Acknowledgments

This work was supported by the National Natural Science Foundation of China (grant numbers 51978330, 51778283); National Natural Science Foundation for the Youth of China (grant number 51808286); Natural Science Foundation of Jiangsu Province (grant number BK20180710); and the Postgraduate Research & Practice Innovation Program of Jiangsu Province (grant number KYCX20_1009). Yi ZENG is grateful for the support of China Scholarship Council (CSC Grant No. 202006250084).

References:

[1] Malhotra PK. Seismic Analysis of Structures and Equipment. Springer Nature Switzerland AG; 2021.

[2] Zhou XY, Yan WM, Yang RL. Seismic base isolation, energy dissipation and vibration control of building structures. Journal of Building Structures 2002; 23: 2-12, 26.

[3] Zhang Y, Ren X, Zhang XY, Huang TT, Sun L, Xie YM. A novel buckling-restrained brace with auxetic perforated core: Experimental and numerical studies. Eng Struct 2021 (Submitted).

[4] Christopoulos C, Pampanin S, Priestley M. Performance-based seismic response of frame structures including residual deformations. Part I: Single-degree of freedom systems. J Earthq Eng 2003; 7: 97-118.

[5] Kiggin S, Uang CM. Reducing residual drift of buckling-restrained braced frames as a dual system. Eng Struct 2006; 28:1525-32.

[6] Ariyaratana C, Fahnestock LA. Evaluation of buckling-restrained braced frame seismic performance considering reserve strength. Eng Struct 2011; 33: 77-89.

[7] Brule S, Enoch S, Guenneau S. Emergence of seismic metamaterials: current state and future perspectives. Phys Lett A 2020; 384: 126034.

[8] Colombi A, Colquitt D, Roux P, Guenneau S, Craster RV. A seismic metamaterial: The resonant metawedge. Sci Rep 2016; 6: 27717.

[9] Krödel S, Thomé N, Daraio C. Wide band-gap seismic metastructures. Extreme Mechanics Letters 2015; 4:

111-7.
[10] Miniaci M, Krushynska A, Bosia F, Pugno NM. Large scale mechanical metamaterials as seismic shields. New J Phys 2016; 18: 083041.
[11] Ren X, Shen J, Tran P, Ngo TD, Xie YM. Auxetic nail: Design and experimental study. Compos Struct 2018; 184: 288-98.
[12] Liu Z, Rumpler R, Feng L. Locally resonant metamaterial curved double wall to improve sound insulation at the ring frequency and mass-spring-mass resonance. Mech Syst Signal Pr 2021; 149: 107179.
[13] Morvan B, Tinel A, Hladky-Hennion AC, Vasseur J, Dubus B. Experimental demonstration of the negative refraction of a transverse elastic wave in a two-dimensional solid phononic crystal. Appl Phys Lett 2010; 96(10): 509.
[14] Zhu R, Liu XN, Hu GK, Sun CT, Huang GL. Negative refraction of elastic waves at the deep-subwavelength scale in a single-phase metamaterial. Nat Commun 2014; 5: 5510.
[15] Muhammad, Lim CW, Reddy JN. Built-up structural steel sections as seismic metamaterials for surface wave attenuation with low frequency wide bandgap in layered soil medium. Eng Struct 2019;188:440-51.
[16] Cheng ZB, Shi ZF. Novel composite periodic structures with attenuation zones. Eng Struct 2013;56:1271-82.
[17] Cheng ZB, Shi ZF, Palermo A, Xiang H, Guo W, Marzani A. Seismic vibrations attenuation via damped layered periodic foundations. Eng Struct 2020; 211: 110427.
[18] Bückmann T, Thiel M, Kadic M, Schittny R, Wegener M. An elasto-mechanical unfeelability cloak made of pentamode metamaterials. Nat Commun 2014; 5: 4130.
[19] Xu L, Wang J, Dai G, Yang S, Yang F, Wang G, et al. Geometric phase, effective conductivity enhancement, and invisibility cloak in thermal convection-conduction. Int J Heat Mass Tran 2021; 165: 120659.
[20] Evans KE, Nkansah MA, Hutchinson IJ, Rogers SC. Molecular network design. Nature 1991;353124.
[21] Lakes R. Foam structures with a Negative Poisson's Ratio. Science 1987; 235: 1038-40.
[22] Zhang XY, Wang XY, Ren X, Xie YM, Zhou YY, Wang SL, et al. A novel type of tubular structure with auxeticity both in radial direction and wall thickness. Thin-Walled Structures 2021; 163: 107758.
[23] Shelby RA, Smith DR, Schultz S. Experimental verification of negative index of refraction. Science 2001; 292: 77-9.
[24] Deymier PA. Acoustic metamaterials and phononic crystals. Berlin: Springer 2013.
[25] Soukoulis CM, Wegener M. Past achievements and future challenges in the development of three-dimensional photonic metamaterials. Nat Photonics 2011; 5: 523-30.
[26] Susstrunk R, Huber SD. Classification of topological phonons in linear mechanical metamaterials. P Natl Acad Sci Usa 2016; 113: E4767-75.
[27] Laude V, Wilm M, Benchabane S, Khelif A. Full band gap for surface acoustic waves in a piezoelectric phononic crystal. Phys Rev E 2005; 71: 036607.
[28] Wang G, Wen X, Wen J, Shao L, Liu Y. Two-dimensional locally resonant phononic crystals with binary structures. Phys Rev Lett 2004; 93: 154302.
[29] Wu TT, Wu LC, Huang ZG. Frequency band-gap measurement of two-dimensional air/silicon phononic crystals using layered slanted finger interdigital transducers. J Appl Phys 2005; 97: 094916.
[30] Zhou XL, Wang LQ. Opening complete band gaps in two dimensional locally resonant phononic crystals. J Phys Chem Solids 2018; 116: 174-9.
[31] Khelif A, Achaoui Y, Aoubiza B. Surface acoustic waves in pillars-based two-dimensional phononic structures with different lattice symmetries. J Appl Phys 2012; 112: 033511.
[32] Khelif A, Achaoui Y, Benchabane S, Laude V, Aoubiza B. Locally resonant surface acoustic wave band gaps in a two-dimensional phononic crystal of pillars on a surface. Phys Rev B 2010; 81: 214303.

[33] Achaoui Y, Antonakakis T, Brule S, Craster RV, Enoch S, Guenneau S. Clamped seismic metamaterials: ultra-low frequency stop bands. New J Phys 2017; 19: 063022.
[34] Liu ZY, Zhang XX, Mao YW, Zhu YY, Yang ZY, Chan CT, et al. Locally resonant sonic materials. Science 2000; 289: 1734-6.
[35] Brule S, Javelaud EH, Enoch S, Guenneau S. Experiments on seismic metamaterials: molding surface waves. Phys Rev Lett 2014;112:133901.
[36] Huang JK, Shi ZF. Application of periodic theory to rows of piles for horizontal vibration attenuation. Int J Geomech 2013; 13: 132-42.
[37] Yan Y, Laskar A, Cheng Z, Menq F, Tang Y, Mo YL, et al. Seismic isolation of two dimensional periodic foundations. J Appl Phys 2014; 116: 044908.
[38] Colombi A, Roux P, Guenneau S, Gueguen P, Craster RV. Forests as a natural seismic metamaterial: Rayleigh wave bandgaps induced by local resonances. Sci Rep 2016; 6: 19238.
[39] Zeng Y, Xu Y, Deng KK, Zeng ZX, Yang HW, Muzamil M, et al. Low-frequency broadband seismic metamaterial using I-shaped pillars in a half-space. J Appl Phys 2018; 123: 214901.
[40] Colquitt DJ, Colombi A, Craster RV, Roux P, Guenneau SRL. Seismic metasurfaces: Sub-wavelength resonators and Rayleigh wave interaction. J Mech Phys Solids 2017; 99: 379-93.
[41] Liu YF, Huang JK, Li YG, Shi ZF. Trees as large-scale natural metamaterials for low-frequency vibration reduction. Constr Build Mater 2019; 199: 737-45.
[42] Du QJ, Zeng Y, Xu Y, Yang H, Zeng Z. H-fractal seismic metamaterial with broadband low-frequency bandgaps. J Phys D-Appl Phys 2018; 51: 105104.
[43] Martelli A, Forni M. Seismic isolation and other antiseismic systems: Recent applications in Italy and worldwide. Seismic isolation and protective systems 2010;175-123.
[44] Zeng Y, Peng P, Du QJ, Wang YS, Assouar B. Subwavelength seismic metamaterial with an ultra-low frequency bandgap. J Appl Phys 2020; 128: 014901.
[45] Shi ZF, Huang JK. Feasibility of reducing three-dimensional wave energy by introducing periodic foundations. Soil Dyn Earthq Eng 2013; 50: 204-12.
[46] Gadallah MR. Applied seismology: a comprehensive guide to seismic theory and application. Pennwell Corp; 2005.
[47] Strek T, Maruszewski B, Narojczyk JW, Wojciechowski KW. Finite element analysis of auxetic plate deformation. J Non-Cryst Solids 2008; 354(35-39): 4475-80.
[48] Grima JN, Caruana-Gauci R, Dudek MR, Wojciechowski KW, Gatt R. Smart metamaterials with tunable auxetic and other properties. Smart Mater Struct 2013; 22: 084016.
[49] Lim TC. Auxetic Materials and Structures. Springer Singapore; 2015.
[50] Lim TC. Mechanics of metamaterials with negative parameters. Springer Nature Singapore Pte Ltd; 2020.
[51] Strek T, Matuszewska A, Jopek H. Finite element analysis of the influence of the covering auxetic layer of plate on the contact pressure. Phys Status Solidi B 2017; 254(12): 1700103.
[52] Jopek H, Strek T. Thermoauxetic behavior of composite structures. Materials 2018; 11(2): 294.
[53] Duc ND, Pharn HC. Nonlinear dynamic response and vibration of sandwich composite plates with negative Poisson's ratio in auxetic honeycombs. J Sandw Struct Mater 2018;20:692-717.
[54] Strek T, Michalski J, Jopek H. Computational analysis of the mechanical impedance of the sandwich beam with auxetic metal foam core. Phys Status Solidi B 2019; 256(1): 1800423.
[55] Bianchi M, Scarpa F. Vibration transmissibility and damping behaviour for auxetic and conventional foams under linear and nonlinear regimes. Smart Mater Struct 2013; 22(8): 84010.
[56] Ungureanu B, Achaoui Y, Enoch S, Brule S, Guenneau S. Auxetic-like metamaterials as novel earthquake

protections. Epj Appl Metamat 2015; 2(17): 1-8.
[57] D'Alessandro L, Zega V, Ardito R, Corigliano A. 3D auxetic single material periodic structure with ultra-wide tunable bandgap. Sci Rep 2018; 8: 2262-9.
[58] Bruggi M, Corigliano A. Optimal 2D auxetic micro-structures with band gap. Meccanica 2019; 54: 2001-27.
[59] Duncan O, Foster L, Senior T, Allen T, Alderson A. A Comparison of Novel and Conventional Fabrication Methods for Auxetic Foams for Sports Safety Applications. Procedia Engineering 2016; 147: 384-9.
[60] Zahra T, Dhanasekar M. Characterisation of cementitious polymer mortar-Auxetic foam composites. Constr Build Mater 2017; 147: 143-59.
[61] Zeng Y, Xu Y, Deng K, Peng P, Yang HW, Muzamil M, et al. A broadband seismic metamaterial plate with simple structure and easy realization. J Appl Phys 2019; 125: 224901.
[62] Auld BA. Acoustic fields and waves in solids, Vol. I. New York: John Wiley&Sons; 1992.
[63] Hofstadter DR. Energy-levels and wave-functions of bloch electrons in rational and irrational magnetic-fields. Phys Rev B 1976; 14: 2239-49.
[64] Park CB, Ryden N, Westerhoff R, Miller RD. Lamb waves observed during MASW surveys. SEG 72nd Annual Meeting 2002.
[65] Wang YC, Lakes R, Butenhoff A. Influence of Cell Size on Re-Entrant Transformation of Negative Poisson's Ratio Reticulated Polyurethane Foams. Cell Polym 2001; 20: 373-85.
[66] Bianchi M, Scarpa F, Smith CW, Whittell GR. Physical and thermal effects on the shape memory behaviour of auxetic open cell foams. J Mater Sci 2010; 45: 341-7.